OP-1

Preparation, Characterization and Application of Styrene Butadiene Rubber (SBR)/ Zinc Sulfide (ZnS) Nanocomposite

V.C Jasna*

Assistant professor, PG Department of Chemistry,

KAHM Unity Women's College, Manjeri, Kerala, India, 676122

Email: jasnavc@gmail.com

Introduction

Over the last few years, nanoparticles have fascinated the academic and industrial community. Nanocomposites, especially polymers as matrix-like elastomers lead to improved mechanical properties, flame retardancy, air, and liquid barrier properties coupled with dimensional and thermal stability. Since they have the potential to replace engineering materials, find use as excellent substitute in construction and automotive sectors. Among the broad variety of nanoparticles available for the development of elastomeric nanocomposites, nanoparticles having specific functional group are desirable due to their novel properties, which further widen their applications [1–4].

Even though, elastomers are good insulators, flexible dielectric composite materials with a high dielectric constant and low dielectric loss tangent are of immense interest at present. Their uses include application as charge storage capacitors, electrostriction artificial muscles and as a materials for controlled drug delivery. Metal oxides or metal sulfide nanoparticles are unique dielectric materials, having excellent thermal stability and therefore number of studies have been carried out to make the polymers thermally stable and conductive, by introducing metal nanoparticles [5,6]. Flame retardancy, thermal stability and electrical properties such as the AC conductivity, dielectric constant and dielectric loss tangent of a polymeric system depend on the nature and amount of metal nanoparticles [7,8]. The increase in AC conductivity of such nanocomposites stems from the formation of a continuous network of nanoparticles in the polymer matrix. These conductive nanocomposite materials are being widely applied in the area of electrostatic discharge dissipation, electro-magnetic interference shielding and other electronic applications [9–11].

ISBN: 978-93-5913-421-5

Among the widely used synthetic elastomers, styrene-butadiene rubber (SBR) deserves a prominent place due to excellent abrasion resistance; thermal and aging stability. SBR is a major and unavoidable component of tyres, cables and insulating materials [12–14]. However, unfilled SBR has poor tensile strength, flame retardancy and oil resistance. The poor tensile strength is due to the absence of strain induced crystallisation and the highly amorphous nature of SBR. The mechanical properties can be improved by the reinforcement of SBR with filler particles, and the novel is by the incorporation of nanoparticles [15–17].

Polymer composites are widely used in the construction and automobile industries. In the automobile industry they serve as oil seals and gaskets. In order to have satisfactory performance, the oil seals should be thermally very stable [18]. During service if they subjected to excess temperature, the material may undergo thermal degradtionand may become soft. Also the contact of these materials with industrail solvents/fuels results in leakage problems and failure in sealing. The study of sorption, diffusion, and permeation in elastomeric nanocomposite provides valuable information about the interaction of the components, the mobility of the chain, and the distribution of organic solvent molecules in polymeric compounds. This study is essential to the successful use of the elastomeric composites in a wide range of applications. The transport properties of nanocomposites strongly depends on the nature of the polymer, the nature of the penetrant, crosslink density and nature of crosslinks, temperature, and the polarity of the matrix [19]. Several works were carried out on the effect of nano-clay on the diffusion and sorption processes [20–22]. However, the studies on the transport of inorganic nanofillers with elastomers are few.

The main purpose of the work is to explore on the insertion of ZnS nanoparticles in SBR to study the interaction between ZnS and SBRand the diffusion and transport properties of SBR/ZnS. The effect of ZnS nanoparticles on the structural properties of SBR was investigated by FTIR and UV spectroscopy. Moreover, the structure and morphology of the composites were examined by XRD and SEM whereas the glass transition temperature and thermogravimetric analysis were examined by DSC and TGA. The diffusion and sorption behavior of both aromatic and industrial solvents through the cross-linked SBR nanocomposite were studied. The dielectric and mechanical properties of the nanocomposites were investigated with respect to various frequencies and volume fractions of nanoparticles.

ISBN: 978-93-5913-421-5

Results and Discussion

FT-IR spectroscopy

Figure 3.1 shows the FT-IR spectra of SBR, ZnS nanoparticles and SBR/ZnS nanocomposites. The characteristic absorption band of SBR is observed at 2910 cm^{-1}, which arise from the CH stretching of phenyl ring. The band centered around1470 cm^{-1} from the C=C modes in the phenyl ring. The absorption at703 cm^{-1} is due to the out-of-plane aromatic ring. The *trans* –CH= mode of butadiene part appeared at 989 cm^{-1} [23]. FT-IR spectrum of ZnS shows an absorption band centered at 3483 cm^{-1}, which is attributed to the O-H stretching vibrations and the HO-H bending vibration (from atmospheric absorbed water) at 1622 cm^{-1}. The main characteristic band of metal sulphide is observed as a broad and strong peak at 615cm^{-1}, which is the typical absorption of ZnS. The SBR/ZnS composite shows the characteristic absorption band of SBR with the typical stretching of metal sulphide. The typical ZnS vibration of composite appears at 609 cm^{-1}, indicating the interaction of nanoparticles with the SBR matrix. Moreover, the stretching vibration of *trans* –CH= group (989 cm^{-1}) in the composite shifts to a lower wave number region (976 cm^{-1}).Hence, it can be inferred that the absorption frequencies of nanocomposite are strongly influenced by the insertion of nanoparticles into the elastomeric matrix [24].

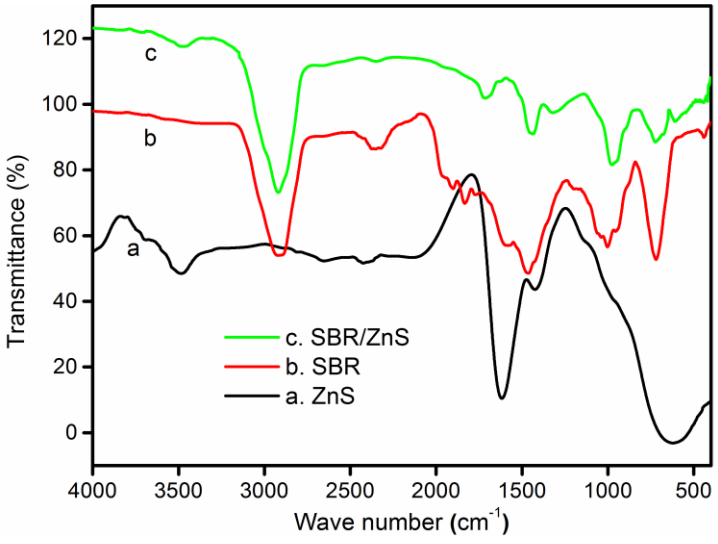

Figure 3.1 FTIR spectra of SBR and ZnS filled SBR

ISBN: 978-93-5913-421-5

UV-Vis Spectra

Figure 3.2 shows the optical properties of SBR and SBR with different contents of ZnS nanoparticles. SBR shows a sharp and prominent peak at 297 nm due to the π-π* transition of the polymer.

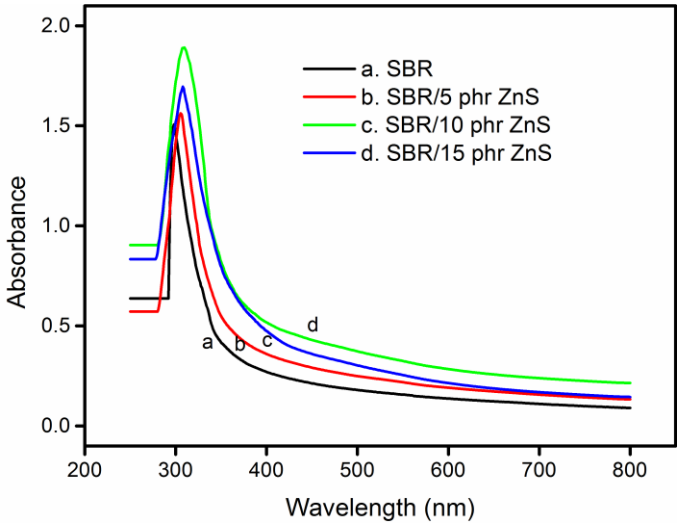

Figure 3.2 UV spectra of SBR with different contents of ZnS nanoparticles

From the UV spectrum of nanocomposite, it can be seen that the characteristic peak of SBR is slightly shifted into a higher wavelength region and the intensity of the absorption peaks of all the composites are higher than that of pure SBR. For example, the sample with 10 phr loading shows a higher UV absorption peak at 309 nm. This suggests that the nanoparticles are uniformly dispersed into the elastomeric matrix which, in turn, increases the interfacial adhesion between the nanoparticles and the SBR chain. It can also be seen from the figure that the absorption edge of nanocomposite is higher than SBR in the entire range of UV absorbance from 200 to 800 nm. The intensity and broadness of the nanocomposite is found to be increasing with the addition of nanoparticles up to 10 phr loading. This means that the interfacial adhesion is the maximum at this loading. The lower absorption edge of the composite beyond 10 phr loading is due to the clustering of nanoparticles in the elastomer and this leads to the poor interaction in the polymer matrix.

X-ray diffraction analysis (XRD)

XRD was used to probe the structure of SBR/ZnS nanocomposites and is displayed in **figure 3.3**. The XRD of ZnS (**Figure 3.3 (e)**) shows that the 2θ values at 28.79, 48.23 and 56.97° are the corresponding crystal plane of (111), (220), and (311) respectively

ISBN: 978-93-5913-421-5

of the cubic phase of ZnS matching with JCPDF 80-0020. The XRD peaks are broadened due to nanocrystalline nature of the synthesised ZnS. No additional peaks are detected for impurities in the sample confirming the phase purity of the synthesised ZnS nanoparticles. The average crystallite size of the powder has been estimated automatically from corresponding XRD data using Scherrer formula, $D=0.94\lambda/\beta\cos\theta$ and the average crystallite size is 2.9 nm. SBR shows a broad peak at $2\theta = 20.17°$ indicating its amorphous nature. It is evident from the figure that the amorphous peak is slightly shifted along with a decrease in the broadness of the peak than that of the corresponding position in pure SBR. For example, the diffraction of 15 phr composite is slightly shifted to a lower diffraction angle from $2\theta = 20.17°$ to 18.76°. The decrease in amorphous nature of SBR with the shift in diffraction angle is assigned to the strong interfacial interaction between the nanoparticles and the elastomeric chain. In order to obtain more structural information, the average crystallite size of ZnS nanoparticles in the composite is calculated from corresponding XRD data and the average size is 16.4 nm [25].

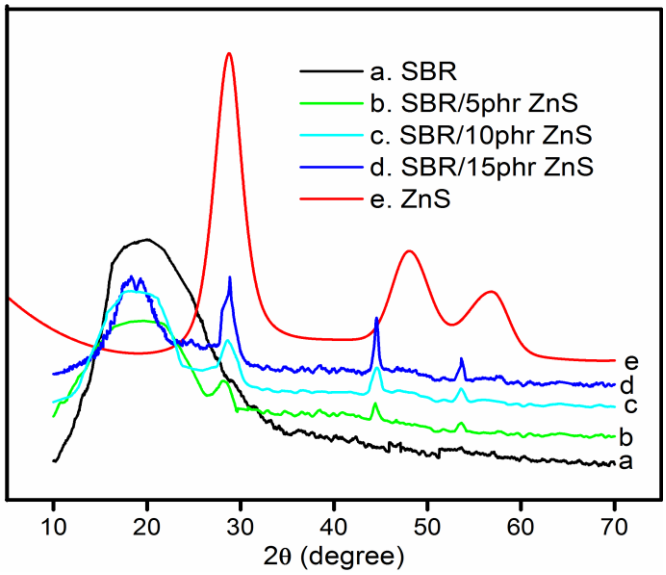

Figure 3.3 XRD pattern of ZnS, SBR and different contents of ZnS filled SBR

Scanning Electron Microscopy (SEM)

The morphological studies of SBR nanocomposite with different contents of ZnS nanoparticles are analysed by SEM and given in **figure 3.4**. The SEM image of SBR (**Figure 3.4 (a)**) presents a smooth and homogeneous structure. However, the inclusion of nanoparticles into the SBR matrix changes the surface morphology of the elastomer

ISBN: 978-93-5913-421-5

composite [26,27]. From **figure 3.4 (b)**, it is clear that the sample with 10 phr of the ZnS particles containing SBR shows a uniform structure with several nanoparticles which are uniformly distributed. The change in the structural morphology of the composite is attributed to the strong interfacial interaction of the SBR phase with the nanoparticles. At 15 phr loading of the nanoparticles (**figure 3.4 (c)**), the surface morphology of the elastomeric composite changes drastically and shows some agglomeration of nanoparticles in the matrix.

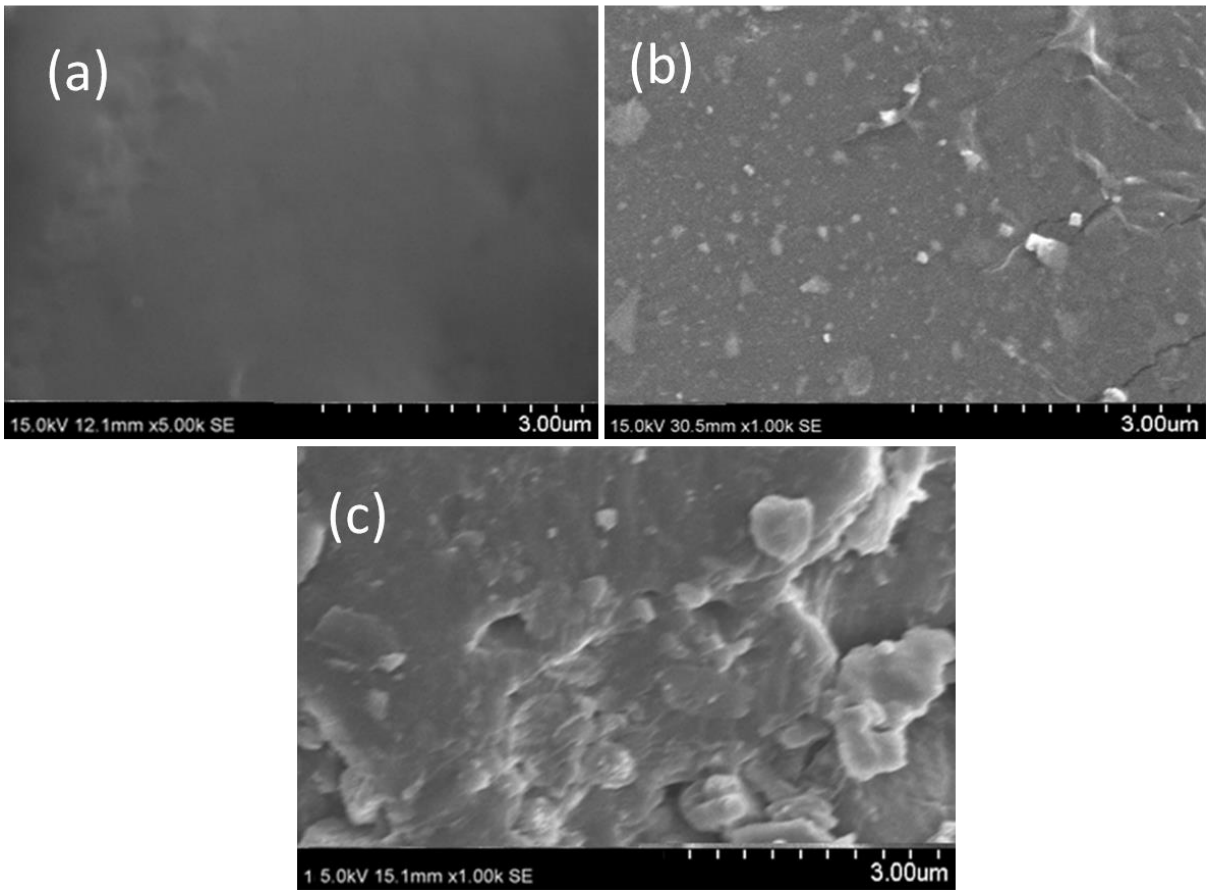

Figure 3.4 SEM pictures of **(a)** SBR **(b)** SBR with 10 phr and **(c)** SBR with 15 phr ZnS
nanoparticles

Thermal properties

Differential scanning calorimetry (DSC)

The DSC profile of SBR and SBR/ZnS nanocomposite with 5, 10 and 15 phr of ZnS nanoparticles is given in **figure 3.5**. It can be seen that the glass transition temperature (T_g) of SBR appears at −56 °C. However, the T_g values of nanocomposite with 5, 10 and 15 phr loading of ZnS nanoparticles are observed at –54.2ºC, –51.3ºC, and –49.1ºC,

ISBN: 978-93-5913-421-5

respectively. Generally, the T_g of elastomeric composite depends on the mobility of the chain, polarity of polymer and filler particles, free volume, and the interaction between filler particles and the macromolecular chain. The high T_g values of nanocomposites, while increasing the loading of nanoparticles, are due to the interfacial interaction between nanoparticles and the macromolecular chain of SBR. In addition to this, the inter-particle distance is short at higher loading, which increases the immobile polymer chain and thereby leads to higher T_g values [28].

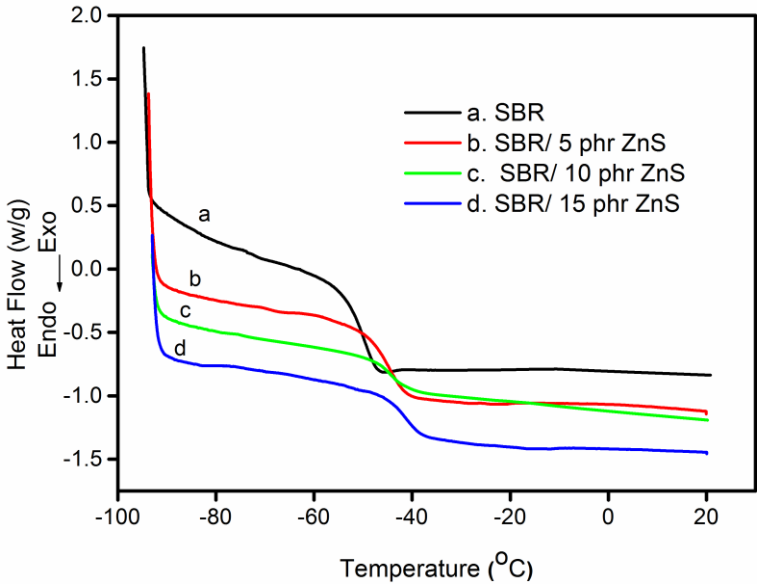

Figure 3.5 DSC thermograms of SBR and SBR with different contents of ZnS nanoparticles

Thermogravimetric analysis (TGA)

The thermal stability of neat SBR and the different contents of ZnS nanoparticles filled SBR at a heating rate of 10 °C min^{-1} is shown in **figure 3.6**. From the figure it can be seen that all samples shows a single step degradation. The onset degradation of SBR is at 401°C which ends around 491°C. The improved thermal stability of SBR/ ZnS nanocomposites is clear from the initial and final temperature of the thermograms. The higher thermal stability of nanocomposites with the increase in concentration of nanoparticle is due to the increased interfacial adhesion between the ZnS nanoparticles and the elastomeric chain. The nanoparticles with a large surface area can strongly reinforce the SBR matrix, producing a protective layer on the surface of SBR and thereby acquire excellent thermal stability. The char residue remaining at 600 °C is 9.61 % for the neat SBR. However, the composites with 5, 10 and 15 phr of nano-ZnS filled SBR show the residue of 14.62, 18.68 and 22.94% respectively at 600 °C.The char

ISBN: 978-93-5913-421-5

layers act as a protective coating on the surface of nanocomposite, which prevents further burning.The higher char residue is an indication of the better thermal and flame resistance of the polymer matrix [29,30]. This broadens the utility of these materials in various applications.

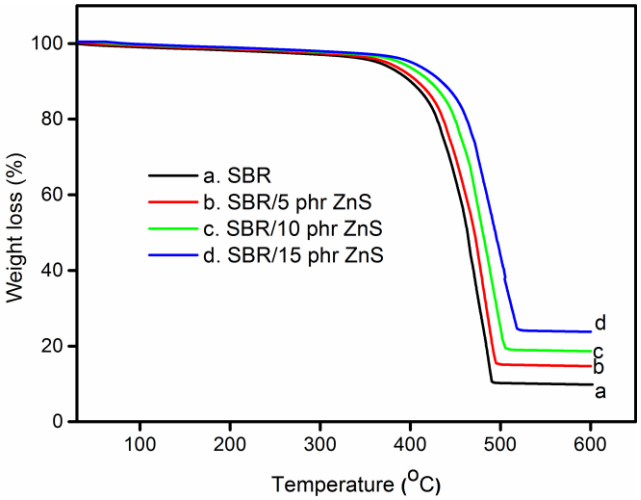

Figure 3.6 TGA curves of SBR and SBR with different contents of ZnS nanoparticles

Cure characteristics

The effect of loadings of ZnS nanoparticles on the rheometer processing characteristics such as cure time and torque values of SBR is presented in **table 3.1**. The scorch time and optimum cure time values decrease with the loading of ZnS nanoparticles in SBR. This shows that the rate of SBR curing increases with the addition of nanoparticles. This is advantages because it can enhance the production rate of elastomer products developed using these materials. As shown in **table 3.1**, the addition of nanoparticles significantly increases the minimum and maximum torque values. The increase in rheometric torque indicates a better polymer-filler interaction. Here the metal sulphide act as co-activators during the chemical vulcanization process, creating better linkages between the molecular chains of rubber by sulfur, which ultimately led to the increase in crosslinking. The composite with 10 phr sample shows the maximum torque value and beyond 10 phr loading, the torque value is found to decrease. At higher loading, greater stress develops in the elastomeric matrix which leads to poor crosslinks between the polymer and ZnS nanoparticles [23].

ISBN: 978-93-5913-421-5

Table 3.1 Processing characteristics of SBR and SBR with different loading of ZnS nanoparticles

Sample code	Cure time, t_{90} (min)	Scorch time, t_2 (min)	Maximum torque (dNm)	Minimum torque (dNm)
SZ_0	15.7	4.8	29	6.9
SZ_3	15.3	4.6	32	7.5
SZ_5	14.6	4.32	35	7.9
SZ_7	14.1	4.05	37	8.0
SZ_{10}	12.8	3.83	40	8.2
SZ_{15}	12.3	3.55	38	8.1

Mechanical properties

The mechanical properties of SBR nanocomposites namely tensile strength, modulus, elongation at break, tear resistance, hardness, abrasion loss, heat build-up and compression set were determined for all nano-filler loadings. The tensile strength, modulus (at 200% elongation) and tear resistance values are greater than pure SBR (**Table 3.2**). The variation in composite tensile properties is more pronounced at 10 phr loading. This means primarily that the nano- ZnS filleracts as a reinforcing filler in SBR and secondarily there is homogeneous dispersion of nanoparticles in the polymer matrix [31]. The slight decrease in tensile strength, modulus and tear strength observed at higher loadings (15 phr), may be due to the agglomeration of ZnS nanoparticles. This fact is supported by the SEM analyses discussed earlier in this work. The elongation at break (EB) given in **table 3.2** shows that the EB decreases with the loading of nanoparticles in all cases and it is well known that a decrease in EB is indicative of higher reinforcement by nanoparticles [19].

ISBN: 978-93-5913-421-5

Table 3.2 Mechanical properties of SBR and SBR with various contents of ZnS nanoparticles

Properties	**Loading of ZnSnanoparticles (phr)**					
	0	**3**	**5**	**7**	**10**	**15**
Tensile strength (MPa)	2.13	3.87	4.65	5.94	7.19	6.63
Elongation at break (%)	425	419	407	390	381	363
Modulus (300%)	1.94	2.94	4.21	5.19	6.99	5.88
Tear strength (kN/m)	18	23	26	29	32	30
Hardness (Shore A)	33	34	35	36	38	40
Heat build-up (°C)	10	10.5	11.9	12.8	14.3	15.8
Compression set (%)	19.8	19.2	18.32	17.44	16.9	16.3
Abrasion loss (mm^3)	66.8	66.6	66.3	66.0	65.5	65.2

Durometer hardness is one of the most commonly used hardness tests for elastomeric materials; it assesses the material resistance to indentation and is widely employed in the elastomer industry. The hardness of the nanocomposite vulcanizates at different filler loadings is shown in **table 3.2**. A progressive increase in the hardness of composite can be seen with the increase in ZnS nanoparticle content, which is again due to the better interaction between SBR matrix and the nano-filler. Abrasion resistance is the material ability to resist the rubbing, scraping or erosion that tends to progressively remove material from its surface. The abrasion resistances of SBR vulcanizates with various loadings of nanoparticles are also given in the same table. The abrasion resistance of the composite increased with an increase in the nanoparticles

ISBN: 978-93-5913-421-5

up to 10 phr loading. The voids or cracks at the growing tip of flaw are arrested by the nano-sized and crystalline ZnS particles which increases the abrasion resistance. The decrease in abrasion resistance beyond 10 phr loading of ZnS can be attributed to the poor interfacial interaction between SBR and the nanoparticles resulting from agglomeration of ZnS. The compression set measurement is used to measure the ability of elastomeric materials to maintain elastic properties even after prolonged compressive stress. Table 2 shows the compression set values of the SBR vulcanizates with different loadings of ZnS nanoparticles. Pure SBR has higher compression set values than nanocomposites and on increasing filler loading the compression set values decreases. A lower compression set is the key property for the rubber industry in sealing applications. Heat build-up is another important property of elastomers, arising from the internal friction in the compounds. From **table 3.2**, it is clear that the heat build-up of the elastomeric composite enhances with the amount of ZnS nanoparticles and thisis mainly due to the higher internal friction resulting from more extensive crosslinking and improved thermal conductivity of the nanocomposites.The magnitude of the increase in heat build-up is higher at 15 phr ZnS loading. The reinforcing effect and higher thermal conductivity of metal sulphide filled compounds is responsible for the high heat build-up value.

Conductivity studies

AC conductivity

The AC conductivity of various concentrations of nano-ZnS filled SBR and unfilled SBR at different frequencies at room temperature is given in **figure 3.7**. The SBR shows minimum electrical conductivity than that of the metal sulphide nanoparticles filled SBR. Owing to the highly amorphous nature of SBR (confirmed from XRD analysis), the macromolecular chains are randomly oriented in the SBR matrix. Therefore, the linkages through grain boundaries are poor, leading to the lower electrical conductivity of the elastomer. The AC conductivity increases continuously with an increase in frequencies for all the samples. This is due to the rapid transport of hopping charge carriers within the polymer matrix and its composites.From the figure, it can be seen that the AC conductivity of the composite greatly increases with the addition of nanoparticles; the composite with 10 phr filler shows the maximum AC conductivity. This indicates the strong interfacial interactions between the ZnS nano-filler particles and the SBR matrix. The interfacial interaction changes the molecular orientation of

ISBN: 978-93-5913-421-5

SBR from a randomly oriented conformation to a well-defined compact structure. It may also be noted that the bulk conductivity of nanocomposites depends on the loading of fillers, filler-rubber adhesion and uniform dispersion of nanoparticles within the polymer matrix [32]. However at a higher concentration of nanoparticles (15 phr) the interfacial adhesion between the polymer and filler decreases due to the high aggregating tendency of nanoparticles. This breaks the formation of effective conducting chains of ZnS nanoparticles and therefore the conductivity is lower at a higher concentration of nanoparticles.

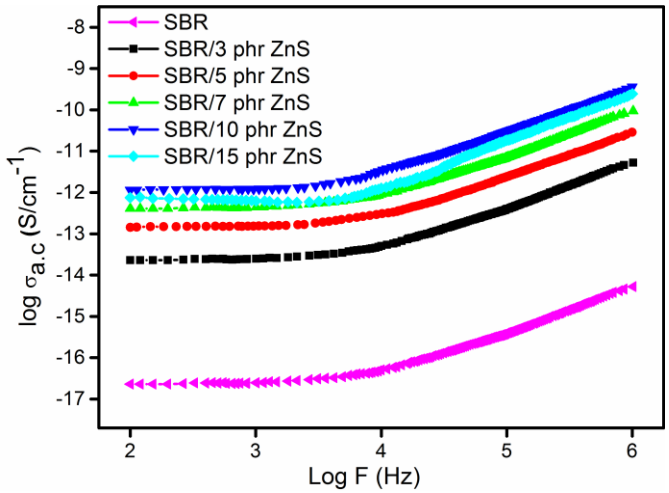

Figure 3.7 AC conductivity of SBR and SBR with different contents of ZnS nanoparticles

Dielectric constant

Figure 3.8 shows the variation of dielectric constant with the frequency of SBR and different loading of ZnS nanoparticles containing SBR. The dielectric constant of polymeric material is directly related to the polarizability of the materials and the interfacial interactions. Also, the presence of aromatic ring, zinc, nitrogen, and sulphur is considered as highly polarisable by the application of an electric field. The dielectric constant of all the composites continuously decreases with an increase in frequency. This is attributed to the tendency of dipoles to orient themselves in the direction of the applied field. The dielectric constant of all the nanocomposites is higher than that of SBR in the entire range of frequencies. In the present study, the higher dielectric constant of the composite is due to the enhanced interfacial interaction between the nanoparticles and the presence of aromatic ring in SBR [33]. The dielectric property of the composite is found to be increasing with the loading of nanoparticles up to 10 phr.

ISBN: 978-93-5913-421-5

When the concentration of nanoparticles reaches to15 phr, the dielectric constant is found to be decreasing. The poor dielectric constant of nanocomposite at higher loading is due to the generation of more and more clusters in the elastomeric matrix (as evident from the UV study).

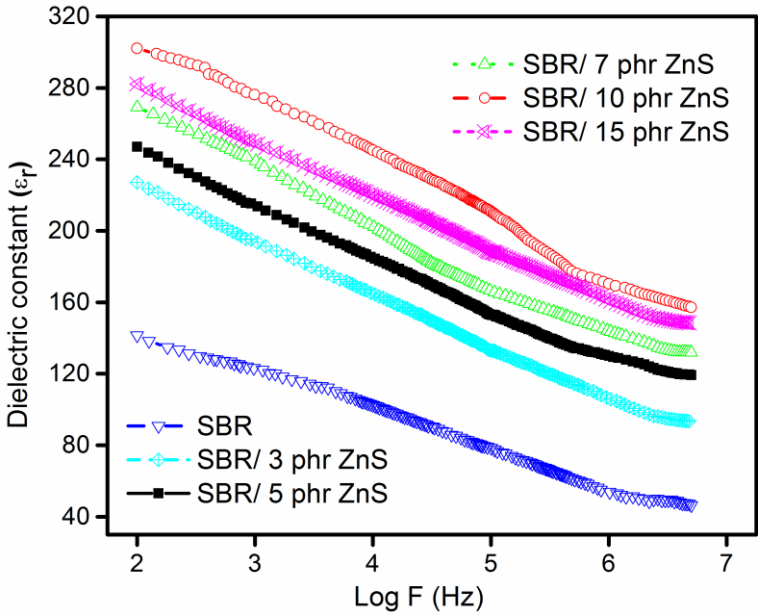

Figure 6

Figure 3.8 Dielectric constant of SBR and different contents of nano-ZnS filled SBR

Dielectric loss (tan δ)

Dielectric loss tangent (tan δ) is the ratio of the electrical energy dissipated in a material to the total power in a circuit. **Figure 3.9** shows the variation of the dielectric loss tangent (tan δ) as a function of frequency ranging from 100-10^6 Hz of SBR and SBR-ZnS nanocomposites at room temperature.It is observed that the tan δ of composite with different contents of nano-filler is higher than that of pure SBR. It is evident that dielectric loss of all the samples decreases steadily with the frequency and reaches a constant tan δ value at 10^4 Hz. This is due to the time lag associated with the orientation of dipoles within the polymer matrix. The tan δ values of SBR/ ZnS nanocomposite is greater than that of the pure SBR. The nanoparticles present in the macromolecular chain of SBR increases the interactions between the components, leading to field distortions and thus an increase in dielectric loss. It is interesting to note that a higher dielectric loss is observed for 10 phr of ZnS, which might be due to the large surface area, surface domain polarisation and the effective electrical network formation [11]. The dielectric loss of the 15 phr loading is lower than that of 10 phr

ISBN: 978-93-5913-421-5

loaded composite. This is due to the formation of clusters or discrete aggregates in the SBR matrix, which prevents charge carriers from migrating through the elastomeric system.

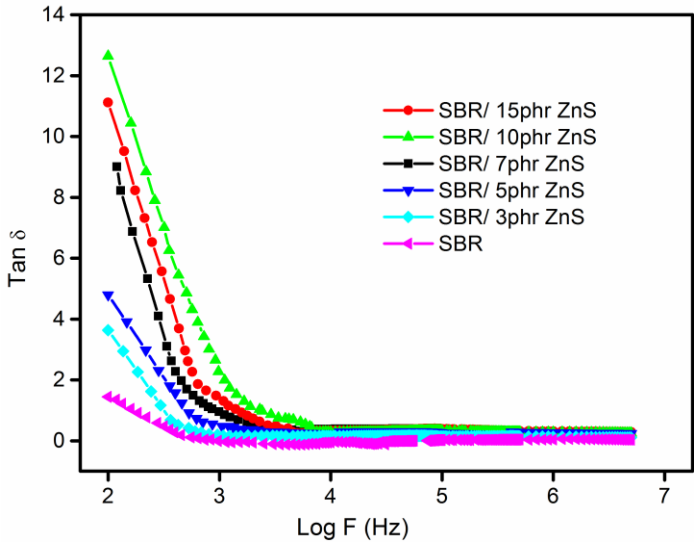

Figure 3.9 Dielectric loss tangent of SBR and different contents of nano-ZnS filled SBR

Analysis of swelling data of aromatic and industrial solvents

Mol % uptake

The mole % uptake of aromatic solvents through SBR/ZnS nanocomposite is studied at room temperature and the mole% uptake of solvent (Qt) was calculated from the **equation 3.1**.

$$Q_t(mol\%) = \frac{mass\ of\ solvent\ sorbed/molecular\ weight\ of\ penetrant}{initial\ weight\ of\ polymer\ sample} \times 100 \quad \textbf{(Eq: 3.1)}$$

The mol % uptake (Q_t %) was plotted against square root of time (√t) in order to get diffusion curves with special reference to the effect of filler loading, effect of solvent and effect of temperature.

Effect of filler loading

The mole % uptakes of benzene and petrol through the SBR with different loading of ZnS nanoparticles are given in **figures 3.10** and **3.11** respectively. It is clear from the figures that the mole uptake progresses first; then it reaches equilibrium and finally becomes constant. It can be seen that, on increasing the ZnS concentrations, the equilibrium sorption decreases and the minimum solvent uptake is observed for the nanocomposite with 10phr of ZnS. This indicates a better polymer-filler interaction,

ISBN: 978-93-5913-421-5

which in turn leads to the decreased flexibility of the polymer chain and the nanocomposite becomes less permeable [34]. On adding filler to the matrix, the free volume inside the matrix decreased, which restricts the free movement of solvent inside the matrix. Thus, upon reinforcement with the filler, the solvent resistance also increases. A better distribution of nanoparticles in the matrix causes an increased surface area of the reinforcing phase, which is the reason for the higher solvent resistance of 10 phr of the composite. However, it is found that, upon further addition of ZnS nanoparticles (above 10 phr), the mole uptake again increases due to the decreased filler-matrix interaction, which leads to the agglomeration of nanoparticles in the SBR matrix. Sorption experiments are found in a similar trend in other two aromatic (toluene and xylene) and industrial (kerosene and diesel) solvents.

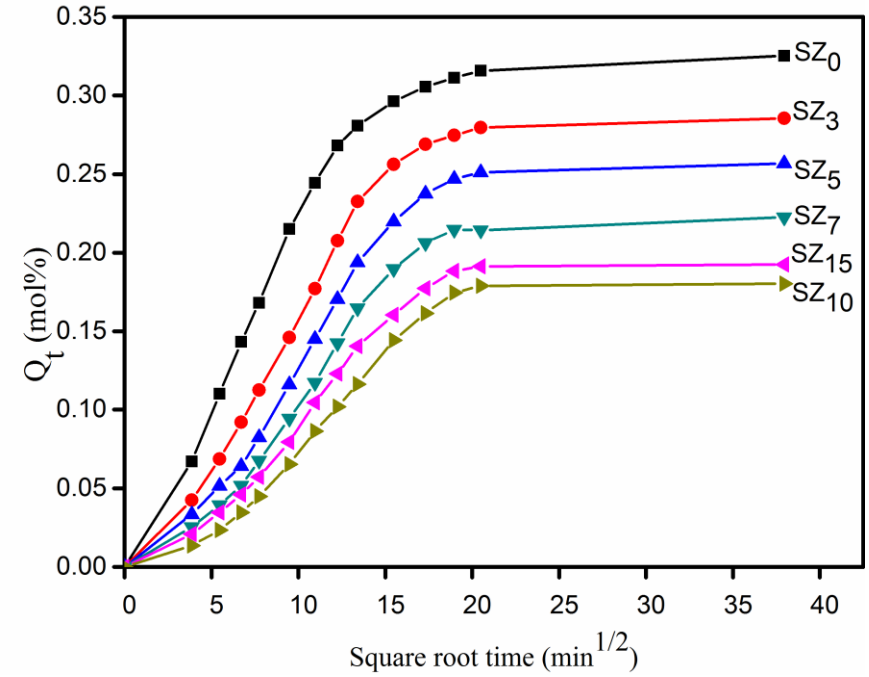

Figure 3.10 mol % uptake of SBR and different contents of nano-ZnS filled SBR in benzene

ISBN: 978-93-5913-421-5

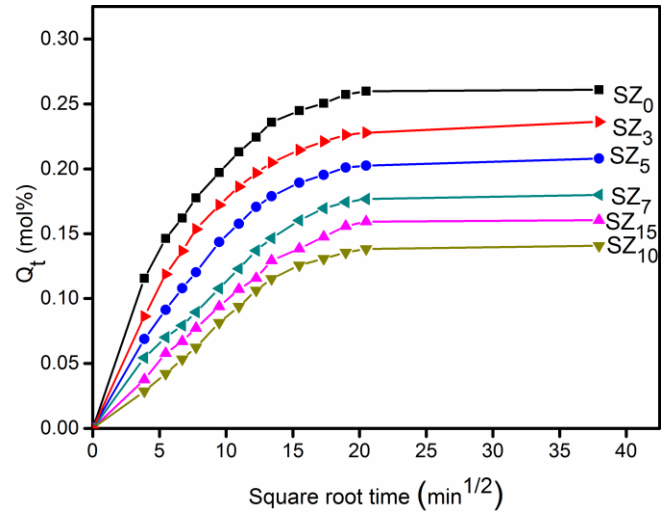

Figure 3.11 mol % uptake of SBR and different contents of nano-ZnS filled SBR in petrol

Effect of penetrant size

The nature of the solvent also affects the mole uptake of the nanocomposite. The transport properties of SBR/ ZnS nanocomposites with 10 phr of ZnS nanoparticles in homologous series of both aromatic and industrial solvents are shown in **figure 3.12** and **3.13** respectively. From the figure it is evident that on increasing solvent density/penetrant size benzene showed highest mol uptake and xylene showed the lowest and the decreasing order is benzene > toluene > xylene. In the case of industrial solvents the order is petrol > kerosene > diesel.

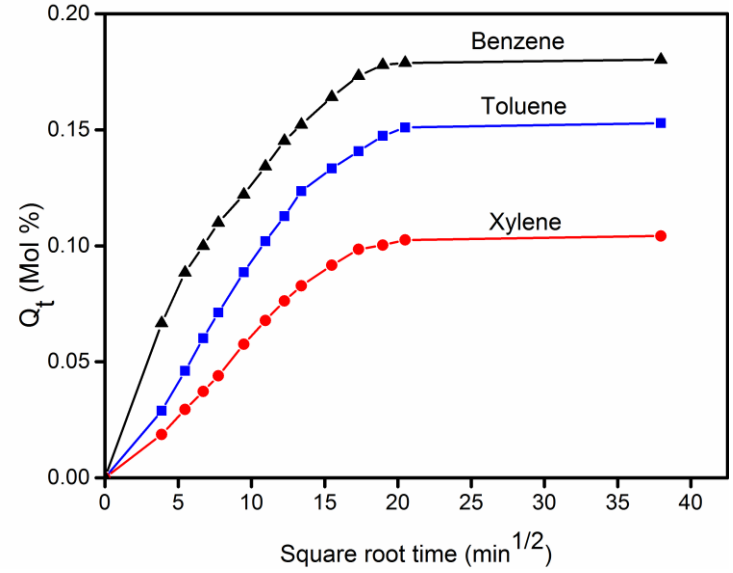

Figure 3.12 Solvent uptake of SBR with 10 phr of ZnS in different aromatic solvents

ISBN: 978-93-5913-421-5

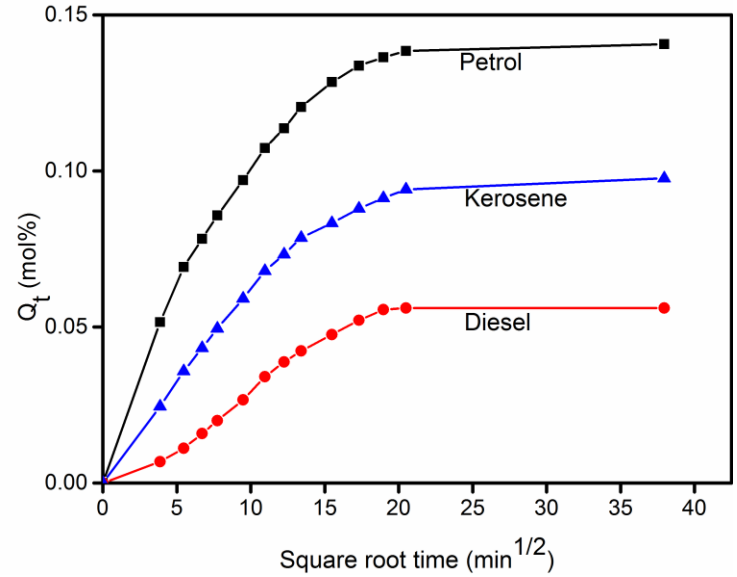

Figure 3.13 Solvent uptake of SBR with 10 phr of ZnS in different industrial solvents

The decrease in solvent uptake on increasing molar volume is reported by many researches. On increasing the molar volume, it needs more space and the exchange become very difficult. It is well established from free volume theory that the increased molar volume will impart restriction on the solvent to enter into the polymer matrix and high activation energy is needed for large molecules to penetrate [35].

Temperature dependence on sorption and diffusion of solvents

The effect of temperature on transport properties of composite is analyzed at different temperatures such as 50 and 70 °C for aromatic solvents and 40 and 50 °C for industrial solvents. **Figure 3.14** depicts the effect of temperature on solvent uptake for SBR/ZnS nanocomposite in benzene and **figure 3.15** in petrol at different temperatures. It can be seen that the solvent uptake of 10 phr nanocomposite is found to be increasing with the temperature. This is mainly due to the increased segmental mobility; as a result, the free volume inside the matrix increases. This again causes the kinetic energy inside the polymer chain to rise [36]. Similar trend is observed for all the samples in all solvents.

ISBN: 978-93-5913-421-5

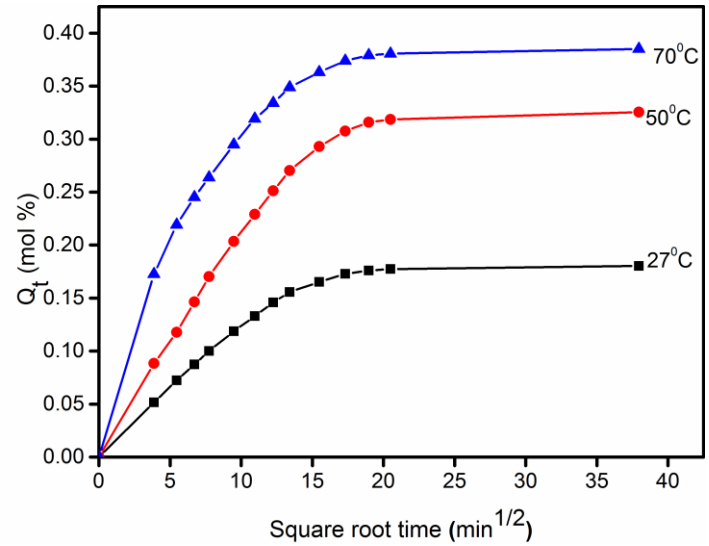

Figure 3.14 The Q_t (mol %) of SBR /10 phr of ZnS in benzene at 27, 50 and 70 °C

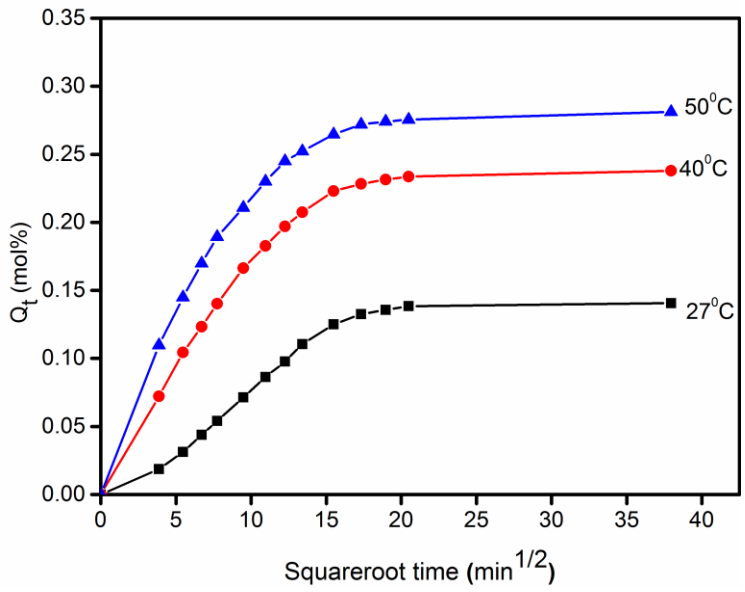

Figure 3.15 The Q_t (mol %) of SBR and SBR /10 phr of ZnS in petrol at 27, 40 and 50 °C

Diffusion (D), sorption (S) and permeation (P) coefficients

The diffusion coefficient (D) is a kinetic parameter, on the basis of segmental mobility which controls diffusion rate. It is calculated using the **equation 3.2**

$$D = \pi\left(\frac{h\theta}{4Q_\infty}\right)^2 \qquad \textbf{(Eq: 3.2)}$$

Where h is the thickness of the sample, θ is the slope of the initial linear region of plot of Q_t versus the square root time and Q_∞ is the equilibrium mol uptake. **Table 3.3** and

ISBN: 978-93-5913-421-5

3.4 clearly demonstrate that the investigations are done for all samples in all three aromatic and industrial solvents. The D values decrease with an increase in concentration of the ZnS nanoparticles up to 10 phr loading. The lowest value of the diffusion coefficient is observed for 10 phr of ZnS containing composite. This is due to the strong interfacial adhesion between the elastomer and nanoparticles. The D value increases upon further addition of filler to the matrix beyond 10 phr. This is because of the agglomeration of nanoparticles cause a decreased interfacial interaction and non-uniform distribution of ZnS filler particles in polymer matrix. Upon increase of penetrant size, diffusivity decreases, petrol shows a higher D value and diesel shows the lowest D value. This is explained on the basis of the free volume theory in terms of the effect of solvent on the mole % uptake of solvent [37,38].

Table 3.3. D, S and P values of SBR/ ZnS nanocomposites in aromatic solvents

Samples	Diffusion coefficient D x 10^5 (cm^2/s)			Sorption coefficient S (mol %)			Permeation coefficient P x 10^5(cm^2/s)		
	Benzene	Toluene	Xylene	Benzene	Toluene	Xylene	Benzene	Toluene	Xylene
S_0	1.81	1.67	1.42	1.20	1.16	1.13	2.17	1.93	1.60
SZ_3	1.79	1.61	1.39	1.18	1.14	1.11	2.11	1.83	1.54
SZ_5	1.77	1.55	1.31	1.17	1.12	1.09	2.07	1.74	1.43
SZ_7	1.73	1.52	1.22	1.15	1.09	1.06	1.98	1.65	1.29
SZ_{10}	1.54	1.37	1.09	1.11	1.05	1.01	1.71	1.43	1.10
SZ_{15}	1.67	1.44	1.13	1.13	1.07	1.03	1.88	1.54	1.16

Table 3.4 D, S and P values of SBR/ ZnS nanocomposites in Industrial solvents

Samples	Diffusion coefficient D x 10^5 (cm^2/s)			Sorption coefficient S (mol %)			Permeation coefficient P x 10^5(cm^2/s)		
	Petrol	Kerosene	Diesel	Petrol	Kerosene	Diesel	Petrol	Kerosene	Diesel
SZ_0	1.51	1.36	1.25	1.21	1.17	1.14	1.81	1.59	1.42
SZ_3	1.38	1.24	1.18	1.19	1.13	1.11	1.64	1.40	1.31

ISBN: 978-93-5913-421-5

S Z_5	1.34	1.18	1.13	1.11	1.07	1.06	1.48	1.26	1.19
SZ_7	1.19	1.13	1.11	1.09	1.03	1.01	1.29	1.16	1.12
SZ_{10}	1.11	0.94	0.88	1.01	0.92	0.88	1.21	0.86	0.77
SZ_{15}	1.14	1.06	1.03	1.07	0.98	0.95	1.22	1.03	0.97

This study observed that the sorption, diffusion and permeation coefficients are highest for petrol and lowest for diesel and intermediate for kerosene. It is explained that smaller molecules will diffuse and get accommodated more easily into the polymer matrix, due to sterric reasons. The decreased sorption values upon increased nano-filler loading can be explained by the fact that the reinforcing materials create obstacles for the penetrating molecules. The bigger the penetrant molecule, the stronger the resistance and hence less will be the penetrant uptake. The Permeation coefficient is the combined effect of the diffusion and sorption coefficients. i.e., P=D.S, the measure of the amount of solvent that permeated per unit area of the sample in one second. Hence it shows a trend similar to that of D and S.

The transport mechanism

The mechanism of transport can be explained from the **equation 3.3**

$$\log \frac{Q_t}{Q_\infty} = \log k + n \log t \qquad \textbf{(Eq: 3.3)}$$

Where Q_t and Q_∞ are the mol % sorption at time t and at equilibrium respectively, k indicates the interaction between the penetrant and the polymer and *n* represents the mode of transport. On regression analysis of $\log \frac{Q_t}{Q_\infty}$ and log t the values of n and k are obtained for aromatic and industrial solvents and these values are given **table 3.5** and **3.6** respectively. From the table it is clear that the value of n is found to be no Fickian first and then on increasing filler loading and solvent size it comes above 0.6 and is nearest to 1. This indicates an anomalous mode of transport and is mainly due to the comparable diffusivity and chain relaxation [39]. The increased swelling stress due to reinforcement is also another reason for the anomalous mode of transport. The value of k proves the structural properties and the increased polymer filler interaction. Generally, the value of k decreases when the distribution of the nanoparticles in the matrix increases. Here , the lowest value for k is noted for 10 phr composite. Upon

ISBN: 978-93-5913-421-5

increasing the penetrant's size, the interaction becomes less and therefore the value of k increases.

Table 3.5 n and k values of SBR/ZnS with different filler loading in aromatic solvents at room temperature

Samples	Benzene		Toluene		Xylene	
	n	$Kx10^2(min^{-1})$	n	$kx10^2(min^{-1})$	n	$Kx10^2(min^{-1})$
S_0	0.51	0.24	0.59	0.15	0.69	0.13
SZ_3	0.53	0.19	0.66	0.13	0.77	0.11
SZ_5	0.59	0.17	0.73	0.11	0.81	0.11
SZ_7	0.67	0.14	0.77	0.10	0.84	0.12
SZ_{10}	0.73	0.11	0.83	0.08	0.88	0.07
SZ_{15}	0.69	0.13	0.79	0.09	0.85	0.11

Table 3.6 n and k values of SBR/ZnS with different filler loading in industrial solvents at room temperature

Samples	Petrol		Kerosene		Diesel	
	n	$Kx10^2(min^{-1})$	n	$kx10^2(min^{-1})$	n	$Kx10^2(min^{-1})$
SZ_0	0.37	0.28	0.49	0.26	0.52	0.22
SZ_3	0.45	0.29	0.56	0.24	0.66	0.21
SZ_5	0.67	0.21	0.62	0.19	0.68	0.17
SZ_7	0.69	0.19	0.66	0.16	0.71	0.14
SZ_{10}	0.77	0.13	0.79	0.12	0.83	0.11
SZ_{15}	0.75	0.15	0.66	0.17	0.72	0.12

Activation energy of diffusion (E_D) and permeation (E_P)

The activation energy of sorption can be calculated from the Arrhenius **equation 3.4**

$$X = X_0 \, exp\left(\frac{-E_X}{RT}\right) \qquad \textbf{(Eq: 3.4)}$$

Where X is D or P, and X_0 is D_0 or P_0. E_x is the activation energy from the plots of log D or logP against 1/T. From the slopes of the curves, the Arrhenius parameters for the samples in aromatic and industrial solvents are obtained and are given in **table 3.7** and **3.8**.

Table 3.7 E_D, and E_P values of SBR-ZnS nanocomposites in aromatic solvents

ISBN: 978-93-5913-421-5

Samples	Benzene		Toluene		Xylene	
	E_P	E_D	E_P	E_D	E_P	E_D
S_0	6.16	4.97	6.39	5.22	6.62	5.43
SZ_3	6.29	5.21	6.51	5.32	6.77	5.51
SZ_5	6.43	5.29	6.62	5.44	6.86	5.57
SZ_7	6.47	5.38	6.64	5.51	6.89	5.62
SZ_{10}	6.54	5.51	6.75	5.67	6.95	5.69
SZ_{15}	6.51	5.44	6.68	5.58	6.90	5.64

The activation energy of diffusion and permeation is found to be increasing with the loading of nanoparticles (**Table 3.7** and **3.8**).The free space in the matrix decreases with increasing filler loading and therefore more energy is needed to obtain free space. Also, on increasing the penetrant's size, the difficulty to enter into the matrix increases and E_P and E_D values increase [40]. Also, the maximum value is for 10 phr composite. A further addition of nanoparticles lowers the activation energy. This is due to the agglomeration of nanoparticles on the surface of polymer or to the decreased interfacial interaction between the rubber and nanoparticles.

Table 3.8 E_D and E_P (kJ mol^{-1}) values of SBR/ZnS nanocomposites in different industrial solvents

Samples	Petrol			Kerosene			Diesel		
	E_D	E_P	ΔH	E_D	E_P	ΔH	E_D	E_P	ΔH
SZ_0	3.59	4.22	0.63	3.97	4.72	0.75	4.62	5.46	0.84
SZ_3	4.49	5.41	0.92	4.54	5.65	1.11	4.63	6.15	1.52
SZ_5	5.92	7.07	1.15	6.18	7.44	1.26	7.08	8.89	1.81
SZ_7	6.08	7.29	1.21	6.32	7.69	1.37	7.19	9.09	1.9
SZ_{10}	6.29	7.54	1.25	6.49	8.36	1.87	7.59	9.64	2.05
SZ_{15}	6.16	7.39	1.23	6.39	7.88	1.49	7.29	9.23	1.94

Thermodynamic parameters

Thermodynamic parameters such as ΔH_s and ΔS_s can be obtained from Van't Hoff's **equation 3.5**

ISBN: 978-93-5913-421-5

$$logK_s = \frac{\Delta S_s}{2.303R} - \frac{\Delta H_s}{2.303RT} \qquad \textbf{(Eq: 3.5)}$$

Where K_s is the equilibrium sorption constant, which is the ratio of the number of moles of solvent sorbed at equilibrium to the mass of the polymer sample. On regression analysis of log Ks against 1/T, the values of ΔH and ΔS are obtained. The thermodynamic properties of SBR and SBR/ZnS composites in aromatic (benzene, toluene and xylene) solvents are given in **table 3.9** while **table 3.10** depicts the thermodynamic parametrers of SBR/ZnS in industrial solvents.

able 3.9 H, S and G of SBR- ZnS nanocomposites in aromatic solvents

Samples	ΔH(J/mol)			ΔS(J/mol/K)			-ΔG(J/mol)		
	Benzene	Toluene	Xylene	Benzene	Toluene	Xylene	Benzene	Toluene	Xylene
S_0	0.871	0.884	0.896	0.071	0.058	0.052	20.43	16.51	14.70
SZ_3	0.877	0.889	0.902	0.068	0.054	0.044	19.52	15.31	12.29
SZ_5	0.882	0.894	0.907	0.065	0.051	0.042	18.61	14.41	11.69
SZ_7	0.889	0.899	0.914	0.061	0.048	0.038	17.41	13.50	10.48
SZ_{10}	0.899	0.912	0.921	0.055	0.041	0.031	15.60	11.39	8.37
SZ_{15}	0.891	0.903	0.917	0.059	0.044	0.034	16.81	12.29	9.28

The positive ΔH value proves the sorption is endothermic. Sorption will occur only by the creation of free space inside the matrix [41]. The reduced entropy on adding filler is due to the decreased interfacial interaction, and is lower in benzene at 10 phr. The value of ΔG also increases upon reinforcement. Among the nanocomposites, 10 phr composite shows the minimum spontaneous sorption which indicates a better interaction between the nanoparticles and the SBR matrix.

Table 3.10 ΔH, ΔS and ΔG (kJ mol^{-1}) values of SBR/ZnS nanocomposites in industrial solvents

Samples	ΔH			ΔS			-ΔG		
	Petrol	Kerosene	Diesel	Petrol	Kerosene	Diesel	Petrol	Kerosene	Diesel
SZ_0	0.635	0.758	0.848	0.068	0.048	0.042	19.77	13.64	11.752
SZ3	0.927	1.117	1.527	0.058	0.044	0.039	16.47	12.08	10.173

ISBN: 978-93-5913-421-5

SZ_5	1.158	1.268	1.817	0.047	0.032	0.029	12.94	8.332	6.883
SZ_7	1.217	1.378	1.979	0.043	0.029	0.022	11.68	7.322	4.621
SZ_{10}	1.258	1.879	2.059	0.029	0.024	0.014	7.44	5.321	2.141
SZ_{15}	1.239	1.497	1.946	0.037	0.026	0.017	9.86	6.303	3.154

Conclusions

The SBR/ZnS nanocomposites were prepared using a simple and environmentally-friendly two-roll mill mixing technique. The composites were characterized by FT-IR, UV, XRD, SEM, DSC, conductivity, and solvent penetration studies. The interaction of nanoparticles with SBR was confirmed from the spectroscopic studies through the shift in absorption peaks of the nanocomposite. The XRD showed the ordered arrangement of filler particles in SBR and the amorphous nature of composite decreased with an increase in content of nanoparticles. The SEM images showed a uniform dispersion of the fillers in SBR. The glass transition temperature of the composites increased with the loading of metal sulphide nanoparticles. TGA results showed increase in thermal stability of nanocomposites upon increasing filler content. The dielectric constant continuously decreased with an increase in frequency for all the systems. The processability, mechanical properties, thermal stability, electrical conductivity and transport behaviour of SBR/ZnS nanocomposites were investigated. Despite the reduction in scorch safety, the compounded SBR/ZnS samples indicated higher production rate resulting from lowering of optimum cure time. Presence of ZnS nanoparticles reduced the amorphous nature of SBR, which is complementary to the enhancement in overall mechanical performance of the composites. A general trend noted was the regular improvement in mechanical properties up to 10 phr loading of ZnS, which dropped with further additions. Mechanical properties such as tensile, tear strength, modulus, hardness, abrasion resistance,heat build-up and compression set were in agreement with the reinforcement by ZnS particles. This is advantages because elastomer nanocomposite with improved mechanical properties tends to be highly performing and durable in service life. Mechanical properties were also supported by the filler distribution analysed by SEM and diffusion studies by using petroleum fuels.

ISBN: 978-93-5913-421-5

The AC conductivity of SBR was significantly enhanced by the addition of ZnS nanoparticles. Dielectric constants of composites were greater than pure SBR and the maximum dielectric value was obtained for 10 phr composite. Diffusion and sorption of aromatic and industrial solvents through SBR/ZnS nanocomposites was studied at different temperatures. The diffusion results were explained in terms of the size of liquid molecules and the diffusion mechanism was found to follow the anomalous in trend. The diffusion and permeation coefficient values decreased with an increase in the molar volume of the solvent. The enhanced dielectric property, solvent resistance, and glass transition temperature of the elastomeric nanocomposites can be used in various applications such as electromagnetic shielding, flexible energy storage and other nanoelectronic devices. To sum up, nano-ZnS acts as a good reinforcement for SBR, especially at 10 phr loading.

1. H. J. Maria, N. Lyczko, A. Nzihou, C. Mathew, S. C. George, K. Joseph, and S. Thomas, J. Mater. Sci. **48**, 5373 (2013).

2. Q. Liu, Y. Zhang, and H. Xu, Appl. Clay Sci. **42**, 232 (2008).

3. V. C. Jasna and M. T. Ramesan, J. Inorg. Organomet. Polym. Mater. **27**, 968 (2017).

4. M. Jacob, K. T. Varughese, and S. Thomas, J. Mater. Sci. **41**, 5538 (2006).

5. K. Suhailath and M. T. Ramesan, J. Mater. Sci. Mater. Electron. **28**, 13797 (2017).

6. H. N. Pazhooh, R. Bagheri, and A. Adloo, Polym. (United Kingdom) **108**, 135 (2017).

7. P. Jayakrishnan and M. T. Ramesan, Polym. Bull. **74**, 3179 (2017).

8. E. Jayamani, S. Hamdan, M. R. Rahman, and M. K. Bin Bakri, Mater. Today Proc. **2**, 2757 (2015).

9. B. Seentrakoon, B. Junhasavasdikul, and W. Chavasiri, Polym. Degrad. Stab. **98**, 566 (2013).

10. M. J. Jiang, Z. M. Dang, and H. P. Xu, Eur. Polym. J. **43**, 4924 (2007).

11. M. T. Ramesan, V. Nidhisha, and P. Jayakrishnan, Mater. Sci. Semicond. Process. **63**, 253 (2017).

12. Y. Zhang, Q. Zhang, Q. Liu, H. Cheng, and R. L. Frost, J. Therm. Anal. Calorim. **115**, 1013 (2014).

ISBN: 978-93-5913-421-5

13. A. Zanchet, L. N. Carli, M. Giovanela, R. N. Brandalise, and J. S. Crespo, Mater. Des. **39**, 437 (2012).

14. L. Guo, G. Huang, J. Zheng, and G. Li, J. Therm. Anal. Calorim. **116**, 359 (2014).

15. H. H. Hassan, E. Ateia, N. A. Darwish, S. F. Halim, and A. K. Abd El-Aziz, Mater. Des. **34**, 533 (2012).

16. S. Mishra and N. G. Shimpi, J. Appl. Polym. Sci. **98**, 2563 (2005).

17. D. Yin, Y. Zhang, R. Fan, and Y. Zhang, Hecheng Xiangjiao Gongye/China Synth. Rubber Ind. **25**, 161 (2002).

18. M. Liu, Z. Jia, D. Jia, and C. Zhou, Prog. Polym. Sci. **39**, 1498 (2014).

19. M. T. Ramesan, Int. J. Plast. Technol. **19**, 368 (2015).

20. Q. T. Nguyen and D. G. Baird, Adv. Polym. Technol. **25**, 270 (2006).

21. B. Xu, Q. Zheng, Y. Song, and Y. Shangguan, Polymer (Guildf). **47**, 2904 (2006).

22. A. Sorrentino, M. Tortora, and V. Vittoria, J. Polym. Sci. Part B Polym. Phys. **44**, 265 (2006).

23. V. C. Jasna and M. T. Ramesan, AIP Conf. Proc. **1849**, (2017).

24. S. Kango, S. Kalia, A. Celli, J. Njuguna, Y. Habibi, and R. Kumar, Prog. Polym. Sci. **38**, 1232 (2013).

25. A. Stroyuk, A. Raevskaya, A. Korzhak, and S. Kuchmii, J. Nanoparticle Res. **9**, 1027 (2007).

26. S. Mitra, S. Chattopadhyay, and A. K. Bhowmick, Polym. Compos. **32**, 103 (2011).

27. L. Flandin, A. Chang, S. Nazarenko, A. Hiltner, and E. Baer, J. Appl. Polym. Sci. **76**, 894 (2000).

28. M. T. Ramesan and T. Sampreeth, J. Mater. Sci. Mater. Electron. 1 (2017).

29. A. Dasari, Z. Z. Yu, Y. W. Mai, and S. Liu, Nanotechnology **18**, (2007).

30. D. W. van Krevelen, Polymer (Guildf). **16**, 615 (1975).

31. T. Johnson and S. Thomas, Polymer (Guildf). **41**, 7511 (2000).

32. M. T. Ramesan and K. Surya, Polym. Compos. (2016).

ISBN: 978-93-5913-421-5

33. K. Suhailath, M. T. Ramesan, B. Naufal, P. Periyat, V. C. Jasna, and P. Jayakrishnan, Polym. Bull. **74**, 671 (2017).

34. S. George, K. T. Varughese, and S. Thomas, Polymer (Guildf). **41**, 579 (2000).

35. C. Sareena, M. T. Ramesan, and E. Purushothaman, Fibers Polym. **14**, 1674 (2013).

36. S. K. Sen, B. Dasgupta, and S. Banerjee, J. Memb. Sci. **343**, 97 (2009).

37. V. C. Jasna and M. T. Ramesan, J. Chem. Pharm. Sci. **2016**–**Janua**, 45 (2016).

38. G. Unnikrishnan, S. Thomas, and S. Varghese, Polymer (Guildf). **37**, 2687 (1996).

39. R. Stephen, K. Joseph, Z. Oommen, and S. Thomas, Compos. Sci. Technol. **67**, 1187 (2007).

40. C. Sareena, M. P. Sreejith, M. T. Ramesan, and E. Purushothaman, Polym. Bull. **72**, 1683 (2015).

41. S. Padhi, P. G. R. Achary, and N. C. Nayak, Bull. Mater. Sci. **38**, 925 (2015).

ISBN: 978-93-5913-421-5